

## SECM Investigation of the Effects of Hydrogen on the Pitting Processes of X70 Carbon Steel in Simulated Soil Solution

Boyu Yuan<sup>1</sup>, Rui Liu<sup>2</sup>, Shuxian Zhao<sup>2</sup>, Liang Li<sup>2</sup>, Chao Wang<sup>2, \*</sup>

<sup>1</sup> Jiangsu Key Laboratory of Advanced Laser Materials and Devices, School of Physics and Electronic Engineering, Jiangsu Normal University, Xuzhou 221116, China

<sup>2</sup> Jiangsu Key Laboratory of Green Synthetic Chemistry for Functional Materials, School of Chemistry & Material Science, Jiangsu Normal University, Xuzhou, 221116, China

\*E-mail: [wangc@jsnu.edu.cn](mailto:wangc@jsnu.edu.cn)

Received: 9 December 2017 / Accepted: 7 February 2018 / Published: 6 March 2018

---

Effects of hydrogen on the dynamic pitting processes of X70 carbon steel in simulated soil solution were investigated by electrochemical methods and scanning electrochemical microscopy (SECM). With increased hydrogen-charged (H-charged) current, corrosion potential shifts negatively and corrosion current increases. A polyaniline microelectrode has been used in SECM to observe the dynamic pH changes at the electrode | electrolyte interface. The results show that decreased pH at the interface corresponds to the occurrence of pitting. It can be concluded that hydrogen is absorbed into the X70 unevenly and reduces interface pH to induce pitting.

---

**Keywords:** X70 carbon steel; Polyaniline-modified Pt microelectrode; H-charged; SECM; Pitting

### 1. INTRODUCTION

X70 carbon steel has been increasingly used in oil and gas pipelines. As a long-distance transportation process, the pipelines are susceptible to damage. Among pipeline failures caused by any single contributor, corrosion is predominant over other factors such as natural force damage, equipment failure, or excavation damage [1]. Among various types of corrosion, pitting is extremely dangerous and destructive due to its rapid propagation and unpredictable nature, making the study of pitting corrosion very important [2-3].

In the past two decades, there has been growing interest in the effect of hydrogen on corrosion [4-17] because the generation and adsorption of hydrogen is unavoidable in many practical processes, such as cathodic protection and acid pickling [5, 6]. It has been found that hydrogen increases the corrosion rate of many kinds of steel [7-17], promotes localized corrosion and decreases stability of the

passive films on iron [4-6]. Moreover, it has also been found that hydrogen decreases the ratio of FeO/Fe in oxide films on the iron surface, which weakens the pitting resistance of the film [6]. The major reactions occurring on the metallic surface are reduction of hydrogen ions and adsorption and diffusion of hydrogen atoms into the bulk metallic phase [8].

SECM, a field observation technology, has obvious advantages of being real-time, *in situ*, and three-dimensional. In addition, it has unique chemical sensitivity: by scanning the Faraday current image of different positions of the substrate with a probe, it can characterize the surface morphology and the electrochemical activity of the substrate electrode [7, 18]. Schaller [19] utilized SECM to map the relative concentration of dissolved hydrogen across an ultrahigh strength stainless steel surface. Xia [20] employed SECM to study the effect of hydrogen on surface reactivity of X80 pipeline steel. It is extremely sensitive in the observation of dynamic pitting processes [21] and has been successfully used to investigate localized corrosion of copper [18], iron [22], aluminium [21,23], zinc [24], and stainless steel [21,25].

Electrodes modified by conducting polymer films have been widely used in analytical chemistry. Among them, electrodes modified by polyaniline derivatives have generated great interest due to their pH response [26-30]. Oyama [27] studied the response of polyaniline-modified electrodes to pH and proposed that the electrodes could be used as pH potentiometric sensors. Jin [28] studied chloroaniline polymer-modified electrodes and found that potential and pH had a linear relationship from pH 2 to 12. Hu [30] studied the electrochemical polymerization of aniline on Pt electrodes and proved that polyaniline-modified electrodes also had good pH response.

In the present work, SECM has been used with Pt microelectrodes with or without polyaniline modification to study the dynamic changes of  $H^+$  (pH) or  $Fe^{2+}$  at the electrode | electrolyte interface during anodic dissolution of X70 electrodes with or without hydrogen charging. The effect of hydrogen on pitting processes is discussed.

## 2. EXPERIMENTAL

### 2.1. Materials and solutions

An X70 carbon steel cylinder ( $d = 2.0$  mm, 0.04% C, 1.46% Mn, 0.003% S, 0.008% P and 0.24% Si) spot-welded to a copper wire and masked with epoxy resin was used as the working electrode (substrate). A platinum disk and saturated calomel electrode (SCE) were used as the counter and reference electrode, respectively. A Luggin capillary was located between the working and reference electrodes to minimize the IR drop. Before each experiment, the working electrode was abraded with emery paper of different grid sizes (600#, 1200#) and then washed with alcohol followed by twice-distilled water. All solutions were prepared using twice-distilled water and analytical-grade reagents. The base solution was simulated soil solution ( $NaHCO_3$ : 0.483 g/L, KCl: 0.122 g/L,  $CaCl_2$ : 0.137 g/L,  $MgSO_4 \cdot 7H_2O$ : 0.131 g/L) [31]. All potentials reported in this work are referred to SCE.

## 2.2. Hydrogen charging

X70 and platinum were used as the cathode and the anode, respectively. Hydrogen charging was carried out at room temperature in 0.5 M Na<sub>2</sub>SO<sub>4</sub> with different current densities ( $i_H = 5 \text{ mA cm}^{-2}$ ,  $10 \text{ mA cm}^{-2}$ ) for 2 h. The X70 electrodes were washed by twice-distilled water immediately between hydrogen charging and the subsequent impedance tests and SECM measurements.

## 2.3. Preparation of the polyaniline-modified Pt microelectrode

In 0.5 M C<sub>6</sub>H<sub>5</sub>NH<sub>2</sub>·HCl + 1.5 M HCl, the Pt microprobe ( $d = 10 \text{ }\mu\text{m}$ ) was used as the working electrode, a platinum disk as the counter electrode, and a SCE as the reference electrode. The Pt microprobe was electrochemically polymerized at 0.7 V for 10 min to produce the polyaniline-modified Pt microelectrode [32]. The  $j_{tip}$ -pH curves of the polyaniline-modified Pt microelectrode were measured in different buffer solutions (pH = 2, 4, 6.86, 8, 9.18).

## 2.4. Electrochemical testing

Potentiodynamic polarization and electrochemical impedance spectra (EIS) were performed by Solartron 1287/1260. The scan rate of the polarization measurements was  $1 \text{ mV s}^{-1}$ . The impedance spectra were obtained in the frequency range from 100 kHz to 10 mHz with 5 mV amplitude of the excitation signal at the open circuit potential.

SECM measurements were performed by CHI910B using a four-electrode system. A Pt microelectrode tip ( $d = 10 \text{ }\mu\text{m}$ ) moved over the substrates, which were immersed in the simulated soil solution. The tip potential was set at +0.6 V [7] to monitor Fe<sup>2+</sup>, while the polyaniline-modified tip potential was set at -1.5 V to monitor pH. The distance between the tip and the substrate was set at 20  $\mu\text{m}$  with the help of a CCD (charge-coupled device). For all SECM measurements, the substrate potential was held 0.1 V higher than the open circuit potential.

Surface morphologies of the specimens were observed using a scanning electron microscope (SEM HITACHI S-3400N) after the electrochemical test.

# 3. RESULTS AND DISCUSSION

## 3.1 Electrochemical measurements

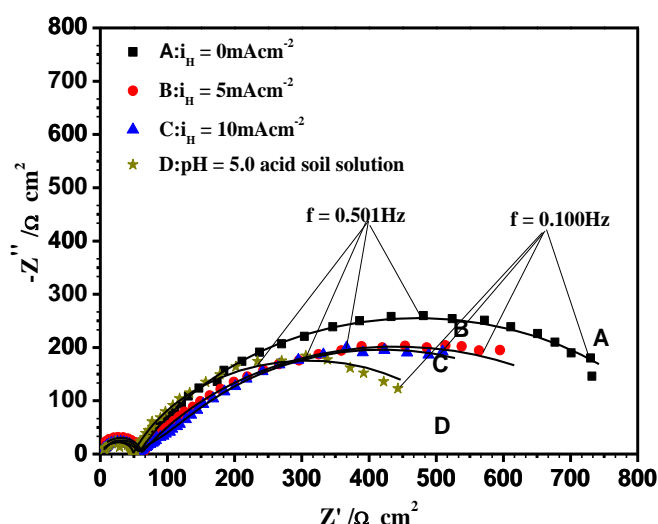
### 3.1.1 EIS measurements

Fig. 1 shows the effects of H-charged current ( $i_H$ ) and pH on EIS of the X70 electrode in simulated soil solution. For the un-charged electrode (pH = 8.2, Fig. 1 A), two depressed capacitive loops are clearly observed. The first loop, observed at high frequencies, may be mainly caused by the double-layer capacitance, while the second loop, observed at low frequencies, can be attributed to both

the charge transfer resistance and the resistance of the surface film. As  $i_H$  increases from 5 (Fig. 1 B) to 10 mA cm<sup>-2</sup> (Fig. 1 C), the radius of the second loop shrinks while the first one remains unchanged, indicating that H-charging decreases the resistance of both the charge transfer and the surface film but has little effect on the value of the double-layer capacitance. When the X70 electrode is charged with hydrogen, hydrogen atoms will be oxidized as shown in the following reactions [5, 7, 33, 34],



The diffused hydrogen atoms are oxidized to H<sup>+</sup> at the metallic surface, which reduces the pH at the electrode | electrolyte interface and increases the ratio of OH<sup>-</sup>/O<sup>2-</sup> in the passive films [5, 7]. Thus, the whole process will undermine the stability of passive films.

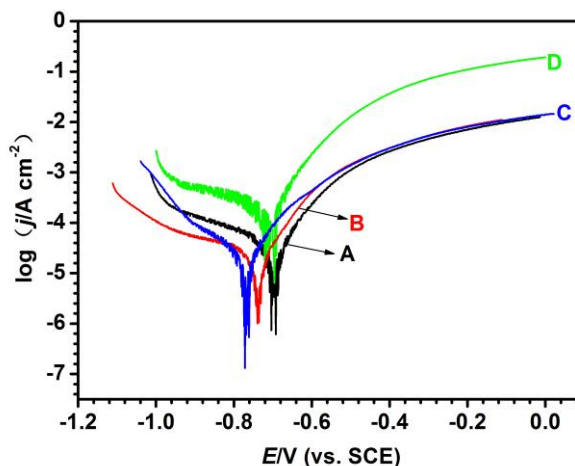


**Figure 1.** Nyquist plots for X70 electrodes at  $E_{ocp}$  in different conditions with 5 mV amplitude of the excitation signal. A, B, C: H-charged X70 in near neutral simulated soil solution, A:  $i_H = 0$  mA cm<sup>-2</sup>; B:  $i_H = 5$  mA cm<sup>-2</sup>; C:  $i_H = 10$  mA cm<sup>-2</sup>; D: uncharged X70 in pH = 5.0 acidic simulated soil solution.

To corroborate the above interpretation, the pH of the simulated soil solution was reduced. As pH decreased from near neutral (Fig. 1 A) to 5 (Fig. 1 D), the impedance spectra remained similar to those of the H-charged specimen, while the radius of the capacitive arch was much smaller. Moreover, the contraction of the real part of impedance appeared at low frequency, indicating the presence of adsorbed intermediates. As a result, local corrosion occurred more readily. The results prove once again that change of pH is the major driving force in the development of corrosion when the electrode is H-charged.

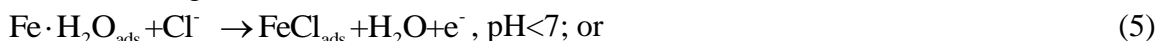
### 3.1.2 Potentiodynamic polarization measurements

Fig. 2 shows the effects of  $i_H$  and pH on the polarization curves of the X70 electrode in simulated soil solution. With the increase of  $i_H$  from 5 (Fig. 2 B) to 10 mA cm<sup>-2</sup> (Fig. 2 C), the anodic current increases compared to that of the un-charged specimen (Fig. 2 A). Table 1 shows the effects of  $i_H$  on the Tafel slopes ( $\beta_a$  and  $\beta_c$ ), the corrosion potential ( $E_{corr}$ ) and the corrosion current ( $j_{corr}$ ). With the increase of  $i_H$ , anodic Tafel slope  $\beta_a$  and  $j_{corr}$  increases while  $E_{corr}$  shifts negatively, indicating that hydrogen enhances the anodic dissolution of the X70 electrode.



**Figure 2.** Polarization curves for X70 electrodes in simulated soil solution with a scan rate of 1.0 mV s<sup>-1</sup>. A, B, C: H-charged X70 in near neutral simulated soil solution A:  $i_H = 0$  mA cm<sup>-2</sup>; B:  $i_H = 5$  mA cm<sup>-2</sup>; C:  $i_H = 10$  mA cm<sup>-2</sup>; D: uncharged X70 in pH = 5.0 acidic simulated soil solution.

To further prove that the change of pH at the interface is the driving force in the corrosion process when the electrode is H-charged, the pH of the solution was reduced. As pH decreased from near neutral (Fig. 2 A) to 5 (Fig. 2 D), the anodic currents increased significantly. The anodic dissolution rate is kinetically controlled by a charge transfer step in the presence of chloride ions as shown in the following reactions [35, 36],



Compared to surface film in alkaline media, a relatively thin and non-uniform product film that has little contribution to the pitting resistance of steel in acidic solution is formed [36].

The effects of pH on  $E_{corr}$  and  $j_{corr}$  are listed in Table 1. Similarly, with a decrease in pH, the corrosion current  $j_{corr}$  increase, while the corrosion potential  $E_{corr}$  shifts negatively, indicating that the effects of hydrogen resemble those of pH on the anodic dissolution of the X70 electrode. The oxidation of hydrogen in the electrode decreased the pH at the electrode | electrolyte interface [7]. Surface films containing more defects become susceptible to electrochemical attacks, thus pitting is more easily initiated and propagated on the surface of the H-charged electrode even in low chloride conditions.

**Table 1.** Corrosion parameters obtained from polarization curves of X70 in simulated soil solution

$i_H$ (mA cm <sup>-2</sup> )	0	5	10	0
pH	8.2	8.2	8.2	5.0
$-E_{corr}$ (V)	0.69	0.74	0.77	0.72
$j_{corr}$ (μA cm <sup>-2</sup> )	0.11	0.13	0.19	0.27

3.2 SECM measurements

3.2.1 SECM measurement of Fe<sup>2+</sup>

As shown in Fig. 3 A1-E1, un-charged X70 is relatively stable in near neutral solution as only one peak appears at 53 min (E1). However, when  $i_H = 5$  mA cm<sup>-2</sup> (A2-E2), two peaks appear at 39 min (D2), which are replaced with two new peaks at 53 min (E2). As  $i_H$  increases to 10 mA cm<sup>-2</sup> (A3-E3), the first peak appears as early as 28 min (C3) and then two new peaks appear at 39 min (D3) while the first one disappears. At 53 min (E3), the number of peaks increases. It is obvious that as  $i_H$  increases, pitting is more easily induced, indicating that hydrogen can accelerate the initiation and the propagation of pitting due to reduction of the pH at the X70 | electrolyte interface.

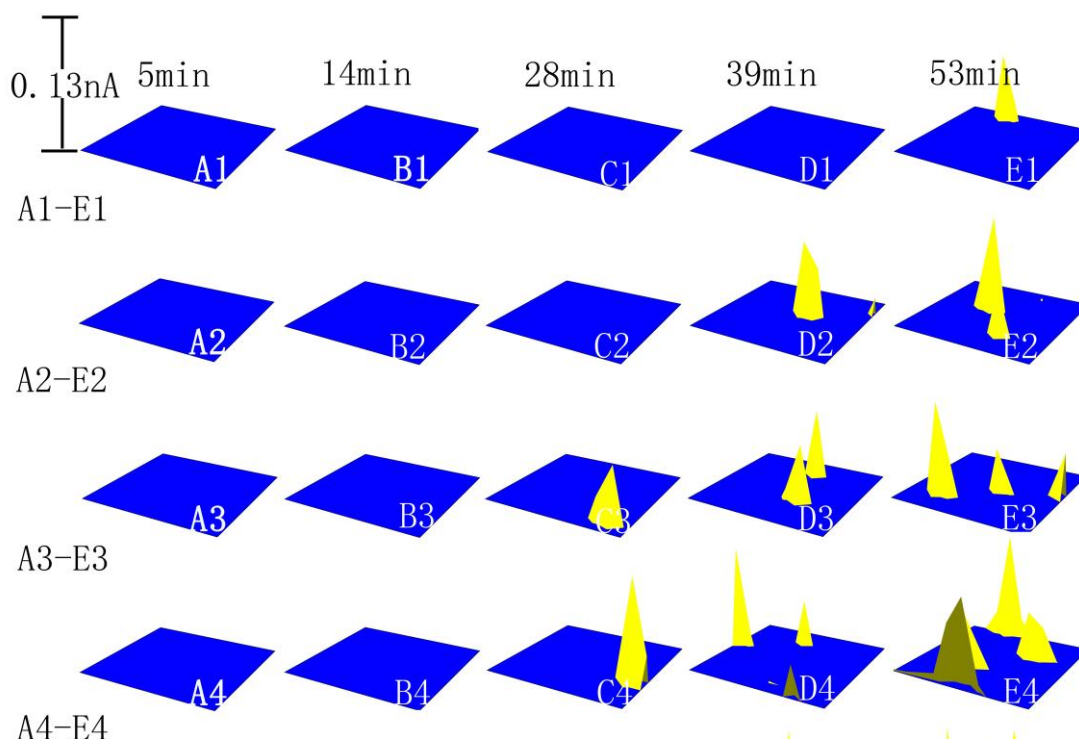


**Figure 3.** SECM images of X70 electrodes polarized at 0.1 V higher than  $E_{ocp}$  in different conditions (200 μm × 200 μm),  $E_{tip} = +0.6$  V (A1-E1, A2-E2, A3-E3: H-charged X70 in near neutral simulated soil solution, A1-E1:  $i_H = 0$  mA cm<sup>-2</sup>; A2-E2:  $i_H = 5$  mA cm<sup>-2</sup>; A3-E3:  $i_H = 10$  mA cm<sup>-2</sup>; A4-E4: uncharged X70 in pH = 5.0 acidic simulated soil solution.)

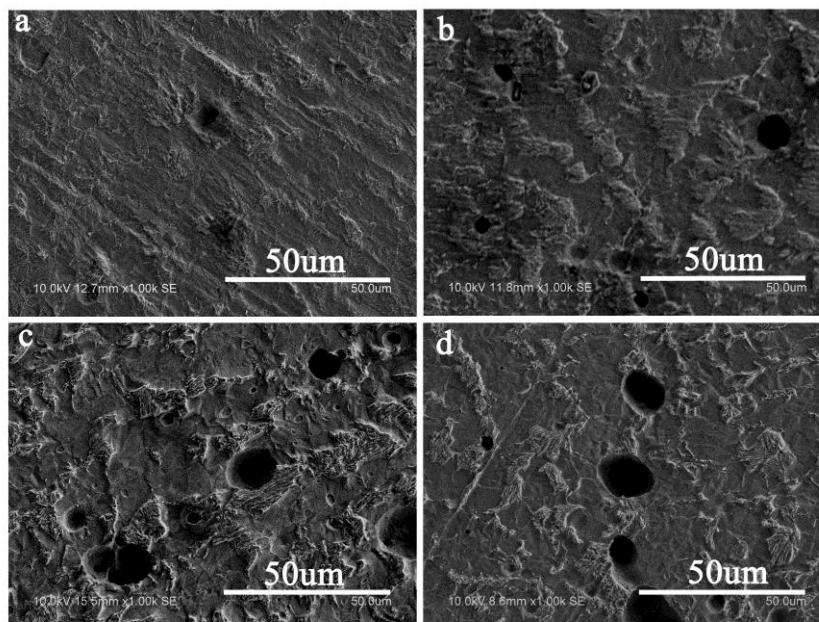


**Figure 4.** SEM images of samples after 1 h polarization at 0.1 V higher than  $E_{ocp}$  in different conditions (a, b, c: H-charged specimens in near neutral simulated soil solution. a:  $i_H = 0 \text{ mA cm}^{-2}$ ; b:  $i_H = 5 \text{ mA cm}^{-2}$ ; c:  $i_H = 10 \text{ mA cm}^{-2}$ ; d: uncharged specimens in pH = 5.0 acidic simulated soil solution.)

When the pH is 5 (Fig. 3 A4-E4), the dynamic processes of pitting are observed successfully. The first peak appears at 28 min (C4). When this peak disappears, three new peaks appear at 39 min (D4), and even more peaks emerge at 53 min (E4). Clearly, either increasing  $i_H$  or decreasing pH of the solution can promote the initiation and propagation of pitting.

Surface morphologies of the samples under different conditions are obtained by SEM (Fig. 4). After 1 h polarization in near neutral simulated soil solution, two pits with small radii are observed (Fig. 4a) on the surface of the uncharged electrode. However, more pits appear on the surface of the H-charged electrode (Fig. 4b,  $i_H = 5 \text{ mA cm}^{-2}$ ) and the number and size of the pits increases with the increase of  $i_H$  (Fig. 4c,  $i_H = 10 \text{ mA cm}^{-2}$ ). The morphology of X70 in acidic solution (Fig. 4d, pH = 5) is similar to that of the H-charged specimen in near neutral solution (Fig. 4c,  $i_H = 10 \text{ mA cm}^{-2}$ ). These results are consistent with those shown in Fig. 3.

Even though the composition of passive film on iron is not known conclusively, it has been reported to be a composition close to  $\text{Fe}_3\text{O}_4$  or  $\gamma\text{-Fe}_2\text{O}_3$ , or a mixture of both [37]. Foley [38] proposed that passive film was  $\gamma\text{-Fe}_2\text{O}_3$  in acidic, neutral and basic solutions; however, the surface films (non-passive films) formed at an active potential was composed only of  $\text{Fe}_3\text{O}_4$ . As shown in Figs. 2-4, the potential (0.1 V higher than  $E_{ocp}$ ) was applied in an active region. It is deduced that the surface film on the X70 electrode is mainly  $\text{Fe}_3\text{O}_4$ . The charged hydrogen reduces the ratio of FeO/Fe in the surface film on the electrode [6], which facilitates the pitting occurrence and propagation. The effect of charged hydrogen is similar to pH reduction on the pitting of the uncharged electrode.

## 3.2.2 SECM measurement of pH

The above results show that the effects of hydrogen have been mainly caused by reduced pH at interface. However, the chemical and physical environment at the interface is different from that of the bulk solution. In other words, pH at the interface is quite different from that of the bulk solution. Therefore, it is not clear whether the effect of hydrogen on the chemical and physical environment at the interface is similar to that of the pH of the solution.

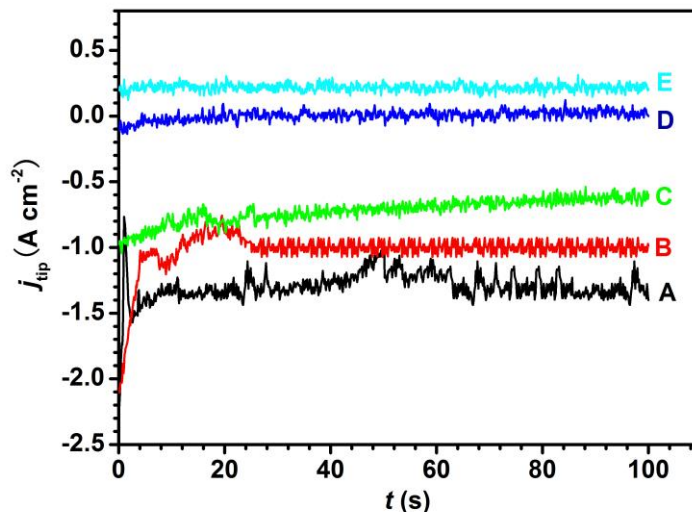


**Figure 5.** The  $j_{\text{tip}}$ -pH curves of polyaniline-modified Pt microelectrode ( $d = 10 \mu\text{m}$ ) in different buffer solutions (A: pH = 2; B: pH = 4; C: pH = 6.86; pH = 8; pH = 9.18.),  $E_{\text{tip}} = -1.5 \text{ V}$ .

It is generally accepted that pH at the electrode | electrolyte interface decreases where pitting occurs [5, 7], so pitting dynamic processes can be observed *in situ* by scanning pH at the interface.

Fig. 5 shows the  $j_{\text{tip}}$ -pH curve of the polyaniline-modified Pt microelectrode in different buffer solutions at tip potential of  $-1.5 \text{ V}$ , which is based on the reduction of hydrogen ions to hydrogen. The lower the pH, the lower the tip current.

Fig. 6 shows the three-dimensional SECM image of  $\text{H}^+$  distribution over the interface. As shown in Fig. 6 (A1-E1), for uncharged X70 in near neutral solution, no obvious pH peaks appear. However, after the electrode is H-charged ( $i_{\text{H}} = 5 \text{ mA cm}^{-2}$ ), the tip current (Fig. 6 A2-D2) slowly decreases from 0 to 39 min and the first pH peak appears at 53 min (Fig. 6 E2), indicating that pitting has occurred. When  $i_{\text{H}} = 10 \text{ mA cm}^{-2}$ , sharp pH peaks emerge at 14 min (Fig. 6 B3) and remain until 28 min (Fig. 6 C3). At 39 min (Fig. 6 D3), all peaks disappear and new ones are not observed until 53 min (Fig. 6 D3). The emergence of pH peaks indicates that the surface of the electrode is not uniform and that hydrogen is absorbed unevenly during the H-charging process. During the pitting process, for H-charged X70 in near neutral solution, the pH peaks can be easily observed because their value in the pitting area is lower than that in the surrounding area.

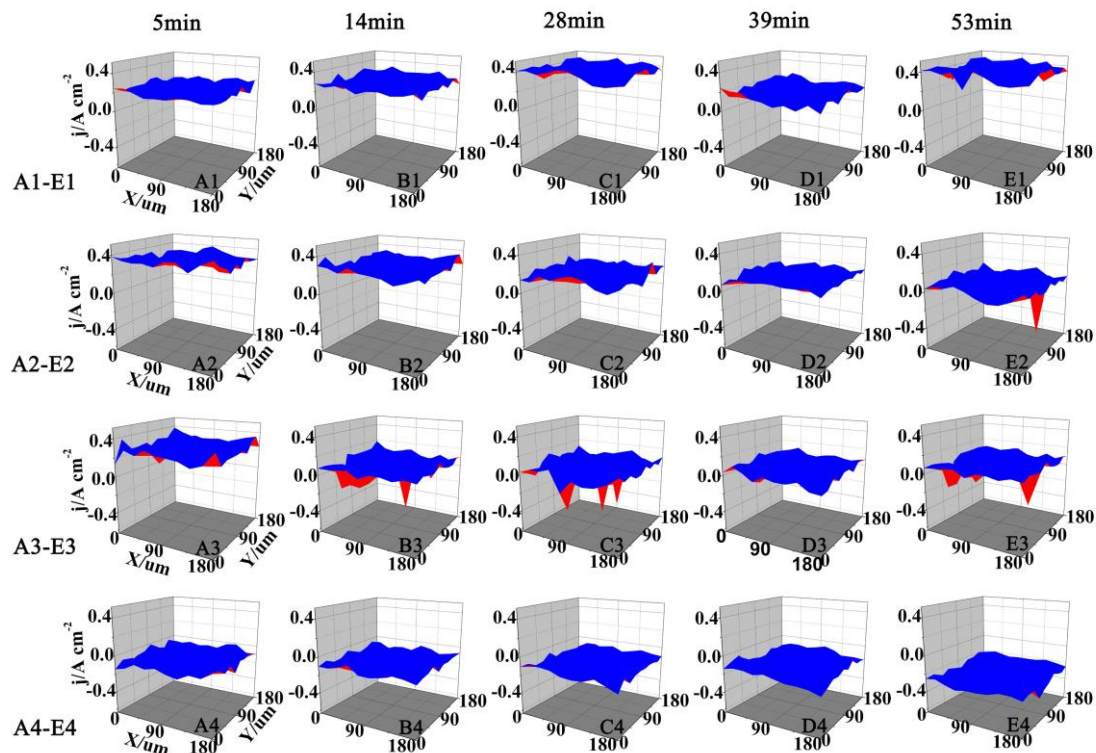


**Figure 6.** pH maps of X70 electrodes polarized at 0.1 V higher than  $E_{ocp}$  ( $200 \mu\text{m} \times 200 \mu\text{m}$  in different conditions,  $E_{tip} = -1.5 \text{ V}$  (A1-E1, A2-E2, A3-E3: H-charged samples in near neutral simulated soil solution, A1-E1:  $i_H = 0 \text{ mA cm}^{-2}$ ; A2-E2:  $i_H = 5 \text{ mA cm}^{-2}$ ; A3-E3:  $i_H = 10 \text{ mA cm}^{-2}$ ; A4-E4: uncharged specimen in pH = 5.0 acidic solution.)

When the pH of the solution is decreased to 5 (Fig. 6 A4-E4), although the reduction current of tip (Fig. 6 A2-E2) decreases, no obvious pH peaks appear, which is quite different from the results shown in Fig. 3 A4-E4. This may be explained as follows: when pitting occurs,  $\text{Fe}^{2+}$  peaks can be observed easily because the concentration of  $\text{Fe}^{2+}$  in the pitting area is higher than that in the surrounding area. However, in contrast to near neutral solution, the pH changes of acidic solution caused by pitting can be hardly detected due to the high concentration of  $\text{H}^+$  in bulk solution; therefore, no obvious pH peaks emerge.

#### 4. CONCLUSIONS

The dynamic processes of pitting and the change in pH at the electrode | electrolyte interface have been studied by SECM combined with electrochemical methods. The following conclusions can be drawn:

(1) The effect of hydrogen is similar to that of reduced pH in promoting the occurrence and the development of pitting.

(2) The dynamic changes in pH at the interface clearly show that hydrogen promotes the occurrence of pitting due to oxidation of the hydrogen, which reduces the pH and the resistance of the oxide film at the interface. The pH decreases where pitting occurs.

(3) In near neutral solution, the H-charged electrode gives rise to local pH peaks, which indicates that hydrogen is unevenly absorbed on the surface of the X70 electrode.

#### ACKNOWLEDGEMENT

This study has been supported by the Chinese National Science Funds (No. 51401094, 21173180, 21473081), project funded by the Priority Academic Program Development of Jiangsu Higher Education Institutions.

#### References

1. I. M. Gadala and A. Alfantazi, *Corros. Sci.*, 82 (2014) 45.
2. L. Zhang, X.G. Li and C.W. Du, *J. Iron. Steel. Res. Int.*, 16 (2009) 52.
3. Y. Li, C. Xu, R. Zhang, Q. Liu, X. Wang and Y. Chen, *Int. J. Electrochem. Sci.*, 12 (2017) 1829.
4. S. Pyun, C. Lim and R. A. Oriani, *Corros. Sci.*, 33 (1992) 437.
5. J.G. Yu, J.L. Luo and P.R. Norton, *Electrochim. Acta*, 47 (2002) 1527.
6. J.G. Yu, J.L. Luo and P.R. Norton, *Electrochim. Acta*, 47 (2002) 4019.
7. Y. Yuan, L. Li, C. Wang and Y.Y. Zhu, *Electrochem. Commun.*, 12 (2010) 1804.
8. Y.M. Zeng, J.L. Luo and P.R. Norton, *Electrochim. Acta*, 49 (2004) 703.
9. L.J. Qiao and J.L. Luo, *Corros. Sci.*, 54 (1998) 281.
10. S.Ningshen, U.KanachiMudali, G. Amarendra, P. Gopalan, R.K. Dayal and H.S.khatak, *Corros. Sci.*, 48 (2006) 1106.
11. Y.H. Huang, F.Z. Xuan, S.T. Tu and T. Itoh, *Mat. Sci. Eng. A-Struct.*, 528 (2011) 1882.
12. L.Q. Guo, Y. Bai, B.Z. Xu, W. Pan, J.X. Li and L.J. Qiao, *Corros. Sci.*, 70 (2013) 140.
13. L. Q. Guo, D. Liang, Y. Bai, X. L. Miao, L. J. Qiao and A. A. Volinsky, *Corrosion*, 70 (2014) 1024.
14. C. Wen, M. Yu, S. Li, X. Li and J. Liu, *Int. J. Electrochem. Sci.*, 9 (2014) 5803.
15. Y. X. Qiao, X. Cai, C. Ouyang and Y. G. Zheng, *Int. J. Electrochem. Sci.*, 11 (2016) 10329.
16. S. Thomas, N. Ott, R. F. Schaller, J. A. Yuwono, P. Volovitch, G. Sundararajan, N. V. Medhekar, K. Ogle, J. R. Scully and N. Birbilis, *Heliyon*, 3 (2017) e00209.
17. S. Thomas, G. Sundararajan, P. D. White and N. Birbilis, *Corrosion*, 73 (2017) 426.
18. C.X. Li, L. Li and C. Wang, *Electrochim. Acta*, 115 (2014) 531.
19. R.F. Schaller, S. Thomas, N. Birbilis and J.R. Scully, *Electrochem. Commun.*, 51 (2015) 54.
20. D. Xia, S. Wu, Y. Zhu, Z. Wang, Y. Sun, R. Zhu and J. Luo, *Electrochemistry*, 84(2016) 238.
21. H. Hao, C. Xu, Y. Li, E. Jackson and X. Shi, *Int. J. Electrochem. Sci.*, 12 (2017) 3732.
22. K. Fushimi and M. Seo, *Electrochim. Acta*, 47 (2001) 121.
23. J. C. Seegmiller and D. A. Buttry, *J. Electrochem. Soc.*, 150 (2003) 413.
24. J.Izquierdo, L.Nagy, S.González, J.J. Santana,G. Nagy and R.M. Souto, *Electrochem. Commun.*, 27 (2013) 50.
25. Y. Gonzalez-Gacria, G.T. Burstein, S. Gonzalez and R.M. Souto, *Electrochem. Commun.*, 6 (2004) 637.
26. B. Lakard, D. Magnin, O. Deschaume, G. Vanlancker, K. Glinel, S. Demoustier-Champagne, B. Nysten, P. Bertrand, S. Yunus and A.M. Jonas, *Sensor. Actuat. B-Chem.*, 166-167 (2012) 794.
27. Y. Ohnuki, H. Matsuda, T. Ohsaka and N. Oyama, *J. Electroanal. Chem. Interfacial Electrochem.*, 158 (1983) 55.

28. L.T. Jin, S.Y. Sun, P.G. He and Y.Z. Fang, *Anal. Chem.*, 17 (1989) 1077.
29. W. R. Heineman and H. J. Wieck, *Anal. Chem.*, 52 (1980) 345.
30. X.Y. Hu and Z.Z. Leng, *Chinese. J. Appl. Chem.*, 7 (1990) 91.
31. G.Z. Meng, C. Zhang and Y.F. Cheng, *Corros. Sci.*, 50 (2008) 3116.
32. Z.S. Yang and Z.X. Zhang, *Chinese. J. Anal. Chem.*, 23 (1995) 1143.
33. Q. Yang and J. L. Luo, *Electrochim. Acta.*, 45 (2000) 3927.
34. L. Li, J. L. Luo, J. G. Yu, Y. M. Zeng, B. T. Lu and S. H. Chen, *Electrochem. Commun.*, 5 (2003) 396.
35. G. W. Ashley and G. T. Burstein, *Corrosion*, 47 (1991) 908.
36. Y. Wang, G. Cheng, W. Wu, Q. Qiao, Y. Li and X. Li, *Appl. Surf. Sci.*, 349 (2015) 746.
37. J. Yu, Effects of hydrogen on the passive film and pitting of iron, (2002), University of Alberta, Edmonton, Canada.
38. C. L. Foley, J. Kruger and C. J. Bechtoldt, *J. Electrochem. Soc.*, 114 (1967) 994.

© 2018 The Authors. Published by ESG ([www.electrochemsci.org](http://www.electrochemsci.org)). This article is an open access article distributed under the terms and conditions of the Creative Commons Attribution license (<http://creativecommons.org/licenses/by/4.0/>).